Hyperbolic chaotic attractor in amplitude dynamics of coupled self-oscillators with periodic parameter modulation

Olga B. Isaeva, Sergey P. Kuznetsov
Kotel'nikov's Institute of Radio-Engineering and Electronics of RAS, Saratov Branch, Zelenaya 38, Saratov, 410019, Russian Federation

Erik Mosekilde
Department of Physics, Technical University of Denmark, 28000 Kgs. Lyngby, Denmark
(Dated: May 31, 2011)

The paper proposes a novel approach to constructing feasible examples of dynamical systems with hyperbolic chaotic attractors based on the successive transfer of excitation between two pairs of self-oscillators, that are alternately active. An angular variable, that measures the relations of the current amplitudes for the two oscillators of each pair, undergoes a transformation in accordance with the expanding circle map during each cycle of the process. We start with equations describing the dynamics in terms of complex or real amplitudes and then examine two models based on van der Pol oscillators. One model corresponds to the situation of equality of natural frequencies of the partial oscillators, and another to a non-resonant ratio of the oscillation frequencies relating to each of the two pairs. Dynamics of all models are illustrated with diagrams indicating the transformation of the angular variables, portraits of attractors, Lyapunov exponents, etc. The uniformly hyperbolic nature of the attractor in the stroboscopic Poincaré map is confirmed for a real-amplitude version of the equations by computations of statistical distribution of angles between stable and unstable manifolds at representative set of points on the attractor. In other versions of the equations the attractors relate presumably to the partially hyperbolic class.

PACS numbers: 05.45.-a, 05.40.Ca

I. INTRODUCTION

Chaotic dynamics in dissipative systems is associated with an object called the strange attractor. Nowadays, the collection of models with strange attractors is very rich, including mathematical examples, as well as models of physical, chemical, biological systems (e.g., [1–7]).

About 40 years ago, mathematical studies focused on a special kind of chaotic attractors – the *uniformly hyperbolic attractors*. Attractors of this type occur in systems of the so-called *axiom A class* and are considered in the *hyperbolic theory* [8–17]. Chaotic nature of dynamics on these attractors is proved rigorously. They possess a property of *structural stability*: the phase space structure, character of dynamics, and its statistical characteristics are insensitive to variation of parameters and functions in the governing equations. Originally, it was expected that the uniformly hyperbolic attractors might be relevant to many physical situations when dynamical chaos occurs [11, 17]. However, as time passed, it became clear that the multiple known concrete examples of chaos do not fit the narrow frames of the early hyperbolic theory. Therefore, efforts of mathematicians were redirected at generalizations applicable to broader classes of systems [13, 16, 19, 20]. Abandoned for a long time and not clarified until recently remains a question at the possible occurrence of the dynamical behavior associated with the uniformly hyperbolic attractors in real-world systems (see discussion in [17, 21]). In the theory of oscillations, since the classic works of Andronov and his school, structurally stable (rough) systems have always been regarded as those subjected to priority research, and as the most important for practice [2, 13, 22]. It seems natural that the same should be the case for systems with structurally stable uniformly hyperbolic attractors. The lack of the real-world examples in this regard is an evident dissonance.

Definitions relating to the hyperbolic theory are most easily formulated in terms of the discrete-time dynamics governed by maps (diffeomorphisms). (If needed to deal with continuous time systems, these definitions can be applied using description in terms of Poincaré map.) An orbit is *uniformly hyperbolic* if at each point of this orbit in the vector space of all possible infinitesimal perturbations V one can define a subspace of vectors V_S decreasing in norm in the evolution forward in time and a subspace of vectors decreasing in reverse time, roughly speaking, exponentially. All vectors in the space V must allow representation as linear combinations of vectors belonging to V_S and V_U, i.e. the vector space V is a direct sum $V = V_U \oplus V_S$. The *uniformly hyperbolic attractors* consist exclusively of orbits of this kind.

Some generalization is *partial hyperbolicity* [16, 20]. In this case, the vector space V is a direct sum $V = V_U \oplus V_S \oplus V_C$ of unstable, stable, and center subspaces. The last subspace, V_C, is associated with perturbations either growing in time more slowly than those relating to V_U or decreasing more slowly than those relating to V_S. Attracting invariant sets consisting exclusively of the partially hyperbolic orbits are called *partially hyperbolic*

attractors.

In textbooks and reviews, examples of the uniformly hyperbolic attractors are traditionally represented by artificial mathematical constructions (see e.g. [8–15, 20]). One is the Smale–Williams solenoid, which can occur in the phase space of maps of dimension 3 or more. Consider a domain in the form of torus and think of it as a plastic doughnut. On one step of the transformation we stretch the doughnut, squeeze it in the transversal direction, fold it to get an M-fold loop ($M \geq 2$), and then insert this loop within the original torus. At each next repetition of the procedure, the number of coils is multiplied by the integer M, and the total volume of the object decreases (because the map is dissipative). In the limit the number of coils tends to infinity, and volume to zero. In the transversal cross sections the object displays a Cantor-like structure. An obvious condition for such an attractor to occur is the presence of an angular variable, that undergoes transformation according to the expanding circle (or Bernoulli) map $\varphi_{n+1} = M\varphi_n$.

The first few examples of feasible continuous-time dynamical systems with attractors of Smale–Williams type in their Poincaré maps were suggested in a number of recent papers by Kuznetsov et al. [23–26]. Here, the role of angular variable was played by the phase of some oscillating process. The systems were composed of two or more oscillators that were activated in alternating manner through transfer of excitation from one oscillator to another with the simultaneous transformation of the phase in accordance with a map of Bernoulli type. The chaotic dynamics revealed itself as a random-like behavior of the carrier signal in the succession of oscillation bursts generated by the system. Computations based on verification of the so-called cone criterion [10–15] confirmed the hyperbolic nature of the attractors [27] and, for a particu1ar model system considered in [23, 27], an accurate analysis based on the technique of computer assisted proof has been performed by Wilczak [28].

Due to their structural stability, one expects systems with hyperbolic attractors to be of particular interest as generators of robust chaos for electronic communication systems, random number generators, and various forms of encryption schemes [29–31].

It is worth noticing, however, that the above examples [23–26] describe specially designed devices rather than systems of natural origin. Search for real-world hyperbolic chaotic attractors and demonstration of their possible significance in, e.g., ecology, physiology and neuroscience, or hydrodynamics remain an interesting and challenging problem [13, 21]. In this perspective it is obviously of interest to broaden our understanding of the type of structures that can be expected to display hyperbolic chaotic attractors.

In this paper we suggest a new approach that is based on the amplitude rather than the phase dynamics of the coupled oscillator systems. Section II explains and illustrates the main idea: In a pair of self-oscillators, fed from a common supply, the relative distribution of amplitudes is characterized by an angular variable. We then compose a system of two such pairs of oscillators that alternatively are driven into the active regime by means of an external parameter modulation. At the same time, the oscillator pairs are coupled so that excitation is transferred from one pair to the other in such a way that the artificially introduced angular coordinate undergoes multiplication by a factor $M = 3$ in each cycle of the external modulation. We demonstrate the hyperbolic character of the observed chaotic attractor through calculation of both the Lyapunov spectrum and the return map over a full modulation period. The return map displays a typical Bernoulli shift character with a slope of 3, and the largest Lyapunov exponent is found to be nearly constant and (within the numerical accuracy) equal to $\ln 3$.

In Sections III and IV we examine the implementation of the above approach in two different versions of four coupled van der Pol oscillators. The first example considers the resonant case where the natural frequencies of all four oscillators are equal. The second example, on the other hand, considers a situation in which strong resonances between the two pairs of oscillators do not occur. As believed, in both cases, the attractors are partially hyperbolic: the systems involve (two, respectively one) neutral (or nearly neutral) variables that do not correspond to expanding or contracting directions. However, the presence of these variables apparently does not affect the roughness of the chaotic attractor.

II. AMPLITUDE DYNAMICS IN TERMS OF ANGULAR VARIABLE AND SIMPLE MODEL WITH THE BERNOULLI-LIKE TRANSFORMATION OF THIS VARIABLE

Consider first a pair of self-oscillatory elements whose energy losses are compensated from a common source, and suppose the equations for the complex amplitudes $a_{1,2}$ read

$$\begin{aligned} \dot{a}_1 &= \tfrac{1}{2}(1 - |a_1|^2 - |a_2|^2)a_1, \\ \dot{a}_2 &= \tfrac{1}{2}(1 - |a_1|^2 - |a_2|^2)a_2. \end{aligned} \tag{1}$$

The saturation of the amplitudes is determined obviously by a condition $|a_1|^2 + |a_2|^2 = 1$. At any given time, the current distribution of energy among the oscillators may be characterized by an angular coordinate θ defined in such way that the amplitudes satisfy the required relation: $|a_1|^2 = \cos^2\theta$, $|a_2|^2 = \sin^2\theta$.

Suppose now that we have *two* such pairs of oscillators, each governed by equations of the type (1), and suppose that they are subjected to periodic parameter modulation produced by same external source in such way that the excitation of the two pairs alternates on successive half-periods of the modulation. In addition, we supplement the equations with terms introducing the pair-wise coupling between oscillators relating to two alternately active subsystems. Concrete form of these additional

terms is selected in such way that the transfer of the excitation on each period of the modulation is accompanied with transformation of the angular coordinate θ according to the expanding circle map. (Hereafter we consider the tripling transformations.) As a consequence, the dynamics of the amplitudes in the system will correspond to the presence of the Smale–Williams type attractor in the stroboscopic map.

Let us consider model equations in terms of the complex amplitudes of the following form:

$$\begin{aligned}
\dot{a}_1 &= \tfrac{1}{2}\left[A\cos(2\pi t/T) - |a_1|^2 - |a_2|^2\right] a_1 + \tfrac{1}{2}\varepsilon b_1, \\
\dot{a}_2 &= \tfrac{1}{2}\left[A\cos(2\pi t/T) - |a_1|^2 - |a_2|^2\right] a_2 + \tfrac{1}{2}\varepsilon b_2, \\
\dot{b}_1 &= \tfrac{1}{2}\left[-A\cos(2\pi t/T) - |b_1|^2 - |b_2|^2\right] b_1 + \tfrac{1}{2}\varepsilon a_1(|a_1|^2 - 3|a_2|^2), \\
\dot{b}_2 &= \tfrac{1}{2}\left[-A\cos(2\pi t/T) - |b_1|^2 - |b_2|^2\right] b_2 + \tfrac{1}{2}\varepsilon a_2(3|a_1|^2 - |a_2|^2).
\end{aligned} \tag{2}$$

Here $a_{1,2}$ and $b_{1,2}$ are the complex amplitudes associated with the two subsystems, each composed of a pair of oscillators fed from a separate common energy source. Due to the counter-phase modulation of parameters controlling the self-oscillations in the subsystems, they become active alternately; A is the magnitude of the modulation, T is the period of the modulation. The terms proportional to the constant ε introduce pair-wise coupling between the oscillators relating to the two subsystems. As explaned below, their concrete form is choosing according to the desired mode of operation.

Suppose in a half-period of activity of the first pair ($A\cos 2\pi t/T > 0$) the variables $a_{1,2}$ are characterized by nearly constant amplitudes corresponding to some θ: $a_1 \sim \cos\theta$, $a_2 \sim \sin\theta$. At the beginning of the activity stage for the second pair ($A\cos 2\pi t/T < 0$), the excitation of the oscillators is stimulated by the coupling terms in the third and the fourth lines of Eqs. (2). From the well-known trigonometric relations, one can see that

$$\begin{aligned}
(|a_1|^2 - 3|a_2|^2)a_1 &\sim (\cos^2\theta - 3\sin^2\theta)\cos\theta = \cos 3\theta, \\
(3|a_1|^2 - |a_2|^2)a_2 &\sim (3\cos^2\theta - \sin^2\theta)\sin\theta = \sin 3\theta.
\end{aligned} \tag{3}$$

Hence, the amplitude ratio for the complex variables $b_{1,2}$ will be determined by the tripled angular variable, 3θ. Next, as the activity stage of the second pair comes to the end, the excitation is transferred back to the first pair. According to the form of the coupling terms in the first and the second equations (2), it occurs without change of the θ variable. So, over the complete period of modulation this variable undergoes the tripling transformation: $\theta_{n+1} \approx 3\theta_n$.

Observe that Eqs. (2) are invariant with respect to two phase shifts, i.e. to the variable changes $a_1, b_1 \to a_1 e^{i\varphi_1}, b_1 e^{i\varphi_1}$ and $a_2, b_2 \to a_2 e^{i\varphi_2}, b_2 e^{i\varphi_2}$, where φ_1 and φ_2 are arbitrary constants. We can, therefore, restrict ourselves to the description of amplitude dynamics exclusively, using the equations in real variables

$$\begin{aligned}
\dot{a}_1 &= \tfrac{1}{2}\left[A\cos(2\pi t/T) - a_1^2 - a_2^2\right] a_1 + \tfrac{1}{2}\varepsilon b_1, \\
\dot{a}_2 &= \tfrac{1}{2}\left[A\cos(2\pi t/T) - a_1^2 - a_2^2\right] a_2 + \tfrac{1}{2}\varepsilon b_2, \\
\dot{b}_1 &= \tfrac{1}{2}\left[-A\cos(2\pi t/T) - b_1^2 - b_2^2\right] b_1 + \tfrac{1}{2}\varepsilon a_1(a_1^2 - 3a_2^2), \\
\dot{b}_2 &= \tfrac{1}{2}\left[-A\cos(2\pi t/T) - b_1^2 - b_2^2\right] b_2 + \tfrac{1}{2}\varepsilon a_2(3a_1^2 - a_2^2).
\end{aligned} \tag{4}$$

(Here we allow the variables $a_{1,2}$ and $b_{1,2}$ to be positive or negative, so the true amplitudes of the oscillators correspond to the absolute values of these variables.)

Next, instead of description of the dynamics in terms of continuous time, one can examine the dynamics in discrete time by means of stroboscopic Poincaré map. In our case, the map $\mathbf{x}_{n+1} = \mathbf{T}(\mathbf{x}_n)$ operates with vectors $\mathbf{x}_n = \{a_1, a_2, b_1, b_2\}_{t=nT}$. Although not derived analyt-

ically, this map can be obtained easily through computations by solving the differential equations over one period T. In the frame of the original equations, the map is eight-dimensional (accounting for the complex nature of the variables $a_{1,2}$ and $b_{1,2}$), but for the real-variable equations (4) it is four-dimensional.

In the discussed mode of operation, according to the above argumentation, one can define an angular variable undergoing tripling on successive iterations. Due to compression of the phase volume along other directions in the four-dimensional state space of the Poincaré map of the model (4), the attractor of this map is expected to be a variant of the Smale–Williams solenoid arising due to the tripling of a number of coils on each next step of the iterations. It will be a uniformly hyperbolic attractor embedded in the state space of the four-dimensional Poincaré map with one-dimensional unstable manifolds and three-dimensional stable manifolds of every point on the attractor.

To illustrate that the model operates in accordance with the above description, let us consider some computational results.

Figure 1 shows time dependences for real amplitudes obtained from numerical simulation of equations (4) at appropriately selected parameter values $T = 10$, $A = 3$, $\varepsilon = 0.06$. Observe the alternating activity of the first and the second pairs of the oscillators. As shown below, the transformation of the angular variable responsible for distribution of the amplitudes in each pair of oscillators corresponds to the Bernoulli type map on each modulation period.

Figure 2(a) shows portrait of attractor of the Poincaré map in projection on a plane of variables relating to one of the alternately exciting subsystems and 2(b) shows a numerically obtained diagram illustrating transformation at successive modulation periods of the angular coordinate responsible for distribution of the amplitudes in each pair of the oscillators constituting the system. The attractor indeed looks like a projection of the Smale–Williams solenoid containing fine structure of filaments. The angular variable was evaluated at successive instants $t_n = nT$ as $\theta_n = \arctan[b_1(nT)/a_1(nT)]$, if $a_1(nT) > 0$, and $\theta_n = \arctan[b_1(nT)/a_1(nT)] + \pi$ otherwise. It may be seen that for the cyclic coordinate θ the expanding circle map as recovered with high accuracy producing just the tripling of the variable: one bypass of the circle for pre-image implies the three-fold bypass for the image.

Evaluation of the Lyapunov exponents for the model (4) is based on simultaneous solution of these equations together with a collection of four linearized variation equations along the reference orbit on the attractor, with Gram–Schmidt orthogonalization and renormalization of the respective perturbation vectors in the course of the procedure (the Benettin algorithm [32]).

In Fig. 3 all four Lyapunov exponents for the Poincaré map are plotted versus the amplitude of slow modulation A for fixed values of the parameters $\varepsilon = 0.06$, $T = 10$ (a), the coupling parameter ε for fixed $A = 3$, $T = 10$ (b) and the period of slow modulation T for fixed $A = 3$, $\varepsilon = 0.06$ (c). Notice how the largest exponent remains almost constant and is close to $\ln 3 = 1.0986...$ in a wide range of the parameter. This agrees well with the approximation based on the Bernoulli tripling map. Such behavior of the largest Lyapunov exponent responsible for the chaotic nature of the dynamics confirms structural stability of the hyperbolic attractor, which evidently persists throughout the whole parameter interval. The other three exponents are all negative and correspond to contraction of the phase volume in directions transversal to the filaments of the Smale–Williams solenoid.

For $A = 3$, $\varepsilon = 0.06$ and $T = 10$ the Lyapunov exponents for the Poincaré map are

$$\begin{array}{ll} \Lambda_1 = 1.095, & \Lambda_2 = -4.172, \\ \Lambda_3 = -7.712, & \Lambda_4 = -10.690. \end{array} \tag{5}$$

and an estimate of the fractal dimension of the attractor in the Poincaré sections by the Kaplan–Yorke formula yields $D = 1 + \Lambda_1/|\Lambda_2| \approx 1.26$. The non-integer value reflects the fractal-like structure of the attractor.

To verify the hyperbolicity of the attractor, we apply the numerical approach suggested e.g. in [33–35]. In this procedure, the angles between the directions of growth of small perturbations are calculated forward and backward in time at points of a reference trajectory. Absence of angles close to zero indicates that the dynamics is hyperbolic. If the angle distribution demonstrates nonzero probability of very small angles, it suggests the presence of tangencies between stable and unstable manifolds and thus implies nonhyperbolicity.

In our case for the Poincaré map of the real-amplitude equations (4), the unstable manifold is one-dimensional, and the stable manifold is three-dimensional; and, the modification of the above method [33–35] was described in [23, 24, 36]. First, we generate a representative orbit on the attractor by computing Eqs. (4) over a sufficiently long time interval. Next, we compute variational equations for perturbations of the orbit forward in time, normalizing the vector $\mathbf{a}(t) = \{\tilde{a}_1(t), \tilde{a}_2(t), \tilde{b}_1(t), \tilde{b}_2(t)\}$ at each integration step to preclude divergence. Then, we compute three replicas of the variation equations with randomly chosen initial conditions backwards in time to find three vectors $\mathbf{b}(t)$, $\mathbf{c}(t)$, and $\mathbf{d}(t)$, performing Gram–Schmidt reorthonormalization of the vectors at each integration step to avoid divergence and predominance of one of the vectors.

At each stroboscopic section $t_n = nT$, the vector $\mathbf{a}_n = \mathbf{a}(t_n)$ defines tangent direction to the unstable manifold and the span of $\{\mathbf{b}_n, \mathbf{c}_n, \mathbf{d}_n\} = \{\mathbf{b}(t_n), \mathbf{c}(t_n), \mathbf{d}(t_n)\}$ corresponds to the tangent subspace to the three-dimensional stable manifold. To evaluate the angle α between the unstable and stable manifolds, we determine a vector $\mathbf{v}_n$ transversal to the stable manifold by solving the set of algebraic linear equations $\mathbf{v}_n \cdot \mathbf{b}_n = 0$, $\mathbf{v}_n \cdot \mathbf{c}_n = 0$, $\mathbf{v}_n \cdot \mathbf{d}_n = 0$. Then, we calculate the angle $\beta_n \in [0, \pi/2]$ from $\cos\beta_n = |\mathbf{v}_n \cdot \mathbf{a}_n|/|\mathbf{v}_n||\mathbf{a}_n|$, and set $\alpha_n = \beta_n - \pi/2$. Figure 4 shows the histogram of the

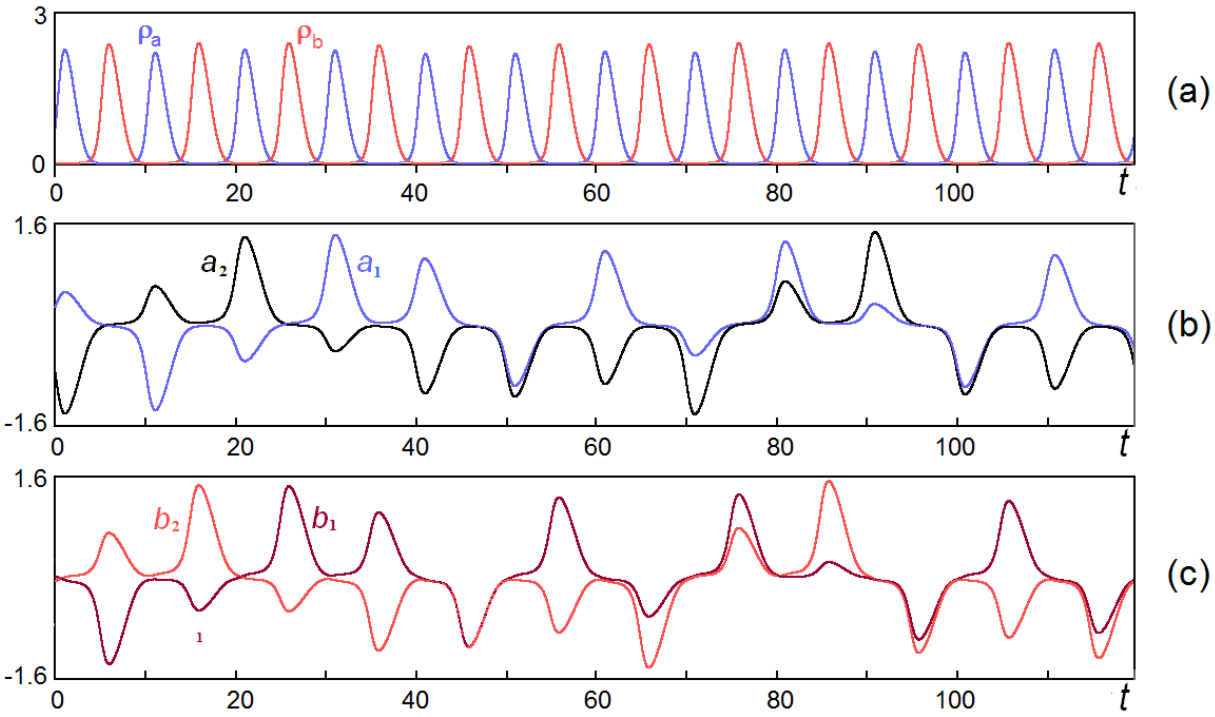

FIG. 1: (Color online) Typical example of time dependences for the amplitude variables of four oscillators obtained from numerical solution of Eqs. (4) with $T = 10$, $A = 3$, $\varepsilon = 0.06$: (a) pair-wise sums of squared amplitudes $\rho_a = a_1^2 + a_2^2$ and $\rho_b = b_1^2 + b_2^2$, and the amplitude variables for the first (b) and the second pair of the oscillators (c).

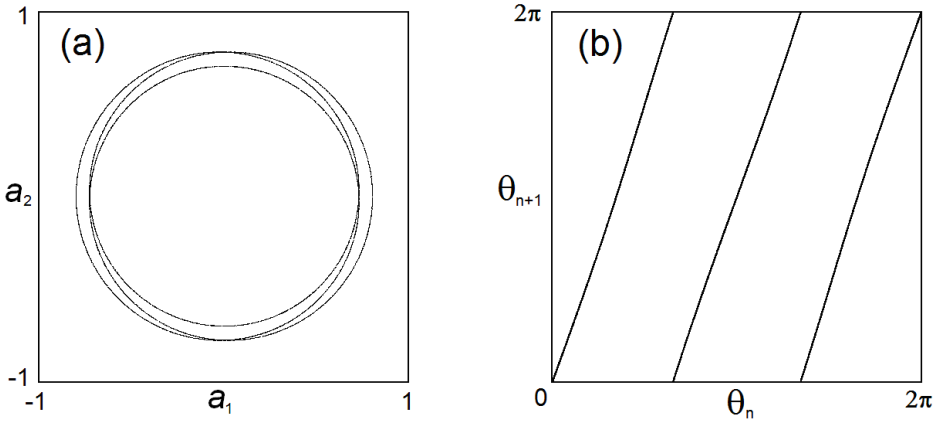

FIG. 2: Portrait of attractor in the Poincaré section in two-dimensional projection on the plane of real amplitudes of the first two oscillators (a) and diagram for the angular variables at successive instants $t = nT$ (b) for the system (4) with $T = 10$, $\varepsilon = 0.06$, $A = 3$.

computed array of α_n. Since the distribution is clearly separated from zero angles, the test confirms the hyperbolicity of the attractor.

For the original set of equations in complex amplitudes (2) evaluation of the Lyapunov exponents in computations yields:

$$\begin{array}{ll} \Lambda_1 = 1.097, & \Lambda_2 = 0.000, \\ \Lambda_3 = 0.000, & \Lambda_4 = -4.166, \\ \Lambda_5 = -5.366, & \Lambda_6 = -5.365, \\ \Lambda_7 = -7.556, & \Lambda_8 = -10.637. \end{array} \qquad (6)$$

The largest exponent is of the same value as in the real-amplitude equations up to numerical errors and it is close to $\ln 3$. The second and the third exponents are zero (up to inaccuracy of the computations); they are evidently associated with the neutral perturbations of the above mentioned two phase shifts leaving the equations invariant. All other exponents are negative; among them Λ_7 and Λ_8 coincide with certain negative exponents from the spectrum of the four-dimensional model, while Λ_5 and Λ_6 are special for the complex-amplitude version of

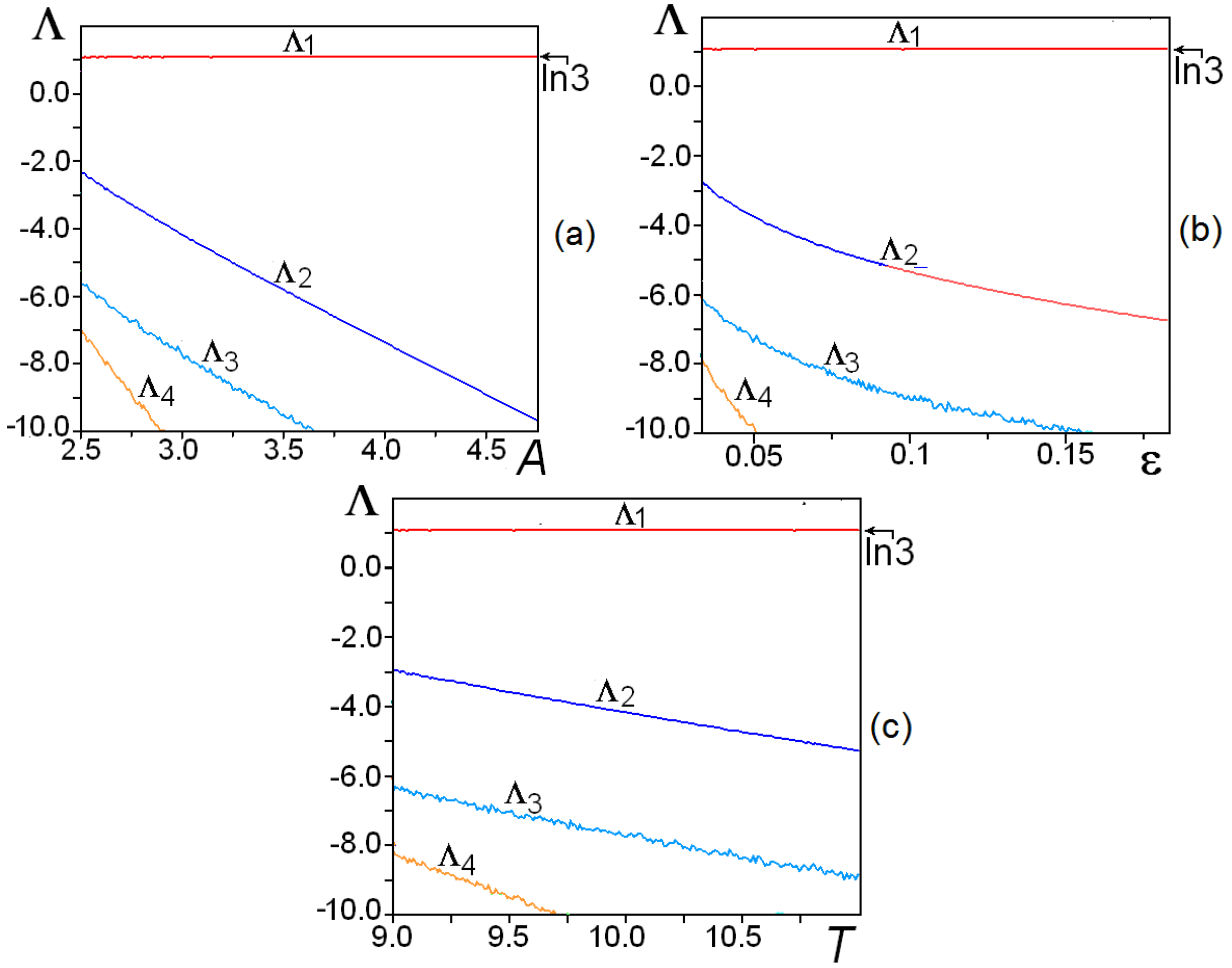

FIG. 3: (Color online) Lyapunov exponents of the Poincaré map for the system (4) plotted versus: (a) the amplitude of the slow modulation A for fixed values of the other parameters $T = 10$, $\varepsilon = 0.06$; (b) the coupling parameter ε for fixed values of the parameters $A = 3$, $T = 10$; (c) the period of the slow modulation T for fixed values of the parameters $A = 3$, $\varepsilon = 0.06$.

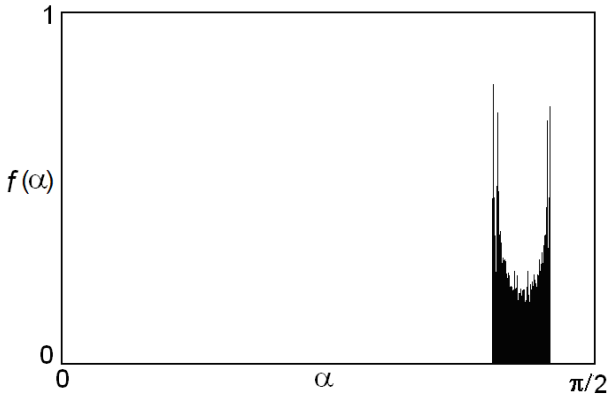

FIG. 4: A normalized histogram for the distribution of angles between the local stable and unstable manifolds for the attractor in the stroboscopic Poincaré map of the model system (4) represented in real amplitudes at $T = 10$, $A = 3$, $\varepsilon = 0.06$. Observe the clearly expressed separation of the distribution from zero angles that is the indicator of the hyperbolicity.

the model.

Estimate of the fractal dimension of the attractor in the Poincaré sections by the Kaplan–Yorke formula yields $D = 3 + (\Lambda_1 + \Lambda_2 + \Lambda_3)/|\Lambda_4| \approx 3.26$. This attractor embedded in the eight-dimensional state space of the Poincaré map has to be regarded as relating to the class of partially hyperbolic attractors because of presence of center subspace associated with the phase variables φ_1 and φ_2 and the corresponding zero-valued two Lyapunov exponents. In the model under consideration this remark is not so essential: the invariance of the equations (2) in respect to the phase shifts is exact; it means that one can accept a rightful agreement not to distinguish states distinct only in the phases, and, in this sense, treat the dynamics as true uniformly hyperbolic. However, in systems, for which description in terms of slow complex amplitudes is approximate (like those discussed in the next two subsections), one may expect peculiarities associated with some features of the partially hyperbolic attractor. If the deflections from the slow-amplitude approximation are small enough, it may be thought that the dynamics of

the amplitude variables will retain its character because of the intrinsic roughness of the hyperbolic attractor.

III. A MODEL OF TWO ALTERNATELY EXCITED PAIRS OF VAN DER POL OSCILLATORS WITH EQUAL NATURAL FREQUENCIES

Let us now turn our attention towards model systems composed of van der Pol oscillators. The van der Pol oscillator is a well known, popular and significant paradigm model of self-oscillatory system. It is often applied in the context of electrical, mechanical, chemical and biological oscillations; and the same may be said in relation to composite schemes based on such elements.

In this section we assume that all partial oscillators used to build a composite system have equal natural frequency ω_0, and consider the following set of equations

$$\begin{aligned}
&\ddot{x}_1 - [A\cos(2\pi t/T) - x_1^2 - x_2^2]\dot{x}_1 + \omega_0^2 x_1 = \varepsilon\dot{y}_1,\\
&\ddot{x}_2 - [A\cos(2\pi t/T) - x_1^2 - x_2^2]\dot{x}_2 + \omega_0^2 x_2 = \varepsilon\dot{y}_2,\\
&\ddot{y}_1 - [-A\cos(2\pi t/T) - y_1^2 - y_2^2]\dot{y}_1 + \omega_0^2 y_1 = \varepsilon(x_1^2 - 3x_2^2)\dot{x}_1,\\
&\ddot{y}_2 - [-A\cos(2\pi t/T) - y_1^2 - y_2^2]\dot{y}_2 + \omega_0^2 y_2 = \varepsilon(3x_1^2 - x_2^2)\dot{x}_2.
\end{aligned} \tag{7}$$

Here we have two pairs of the self-oscillators. Each pair, characterized by the generalized coordinate variables $x_{1,2}$ and $y_{1,2}$, respectively, is supposed to get supply from the common source, as seen from the structure of the expressions in square brackets. The two pairs become active in turn because of the periodic modulation of the parameters responsible for the Andronov–Hopf bifurcation in the van der Pol oscillators; the intensity of the modulation is characterized by parameter A, and its period by the constant T. The coupling terms proportional to the constant ε ensure transfer of the excitation between the first and the second oscillators of each pair; their structure is similar to that postulated in the previous section. Note that the transfer of the excitation occurs under a resonance condition on the natural frequencies of the oscillators through the first harmonic component of the right-hand terms in the equations.

As shown in Appendix, using the approximation of the slow-amplitude approach [2, 22, 40, 41], the system is reduced just to the form, which corresponds to the real amplitude equations (4). Hence, its operation must be similar to that considered in the previous section. In view of the structural stability of the hyperbolic attractor of the model (4), the approximate correspondence is expected to take place, at least for parameters in the range of applicability of the description in terms of the amplitude equations.

Figure 5 shows waveforms generated by the system as obtained from numerical solution of Eqs. (7) for $A = 3$, $T = 10$, $\varepsilon = 0.06$, $\omega_0 = 2\pi$. Panels (a) and (b) represent the plots for the pair-wise coupled oscillators. Observe that the first and the second subsystems are active alternately, and that the distribution of the intensity of the oscillations varies drastically between successive stages of activity. The panel (c) shows the waveforms of two oscillators relating to one and the same subsystem; observe that the phases of both oscillators are the same, at least as distinguishable from the plot. (Actually, this phase varies slowly on large time scales and represents a special variable not involved in the hyperbolic structure; due to this circumstance the attractor in the stroboscopic map of this system should presumably be related to a partially hyperbolic class rather than the uniformly hyperbolic in usual sense.)

It is again convenient to introduce a description in terms of a stroboscopic Poincaré map. Now, the map $\mathbf{x}_{n+1} = \mathbf{T}(\mathbf{x}_n)$ operates with vectors $\mathbf{x}_n = \{x_1, u_1, x_2, u_2, y_1, v_1, y_2, v_2\}_{t=nT}$, where $u_{1,2} = \dot{x}_{1,2}/\omega_0$ and $v_{1,2} = \dot{y}_{1,2}/\omega_0$ are normalized generalized velocities for the respective oscillators. The Poincaré map can be obtained computationally by solving the differential equations (7) for one period T.

To proceed, we need to introduce an angular variable characterizing the distribution of amplitudes for the oscillators constituting one subsystem, expressed via the dynamical variables $(x_{1,2}, u_{1,2})$. In the context of the present model this is more subtle matter than that in the previous section. (A straightforward definition like $\arctan\left[\sqrt{x_2^2+u_2^2}/\sqrt{x_1^2+u_1^2}\right]$ is not satisfactory as it deals with only one of four quadrants for the angular variable. To illustrate the relation to the Smale–Williams solenoid the angular variable needs to be allowed to take values corresponding to the entire circle.) The following approach is found to be successful. First, select a pair from (x_1, u_1) and (x_2, u_2) with larger $r_i^2 = x_i^2 + u_i^2$. Then, if $|x_i| > |u_i|$, we set $s = \mathrm{sgn}(x_i)$, otherwise, $s = \mathrm{sgn}(u_i)$, and $\xi = sx_i/r_i$, $\eta = su_i/r_i$. Now, before and after each step of the Poincaré map, evaluate $X = \xi x_1 + \eta u_1$, $Y = \xi x_2 + \eta u_2$ and $X' = \xi x_1' + \eta u_1'$, $Y' = \xi x_2' + \eta u_2'$, where the prime marks the updated variables. (The coefficients ξ and η are accepted to be identical in the course of evaluation both of X, Y and X', Y'.) Finally, set $\theta = \arg(X + iY)$ and $\theta' = \arg(X' + iY')$ to plot along

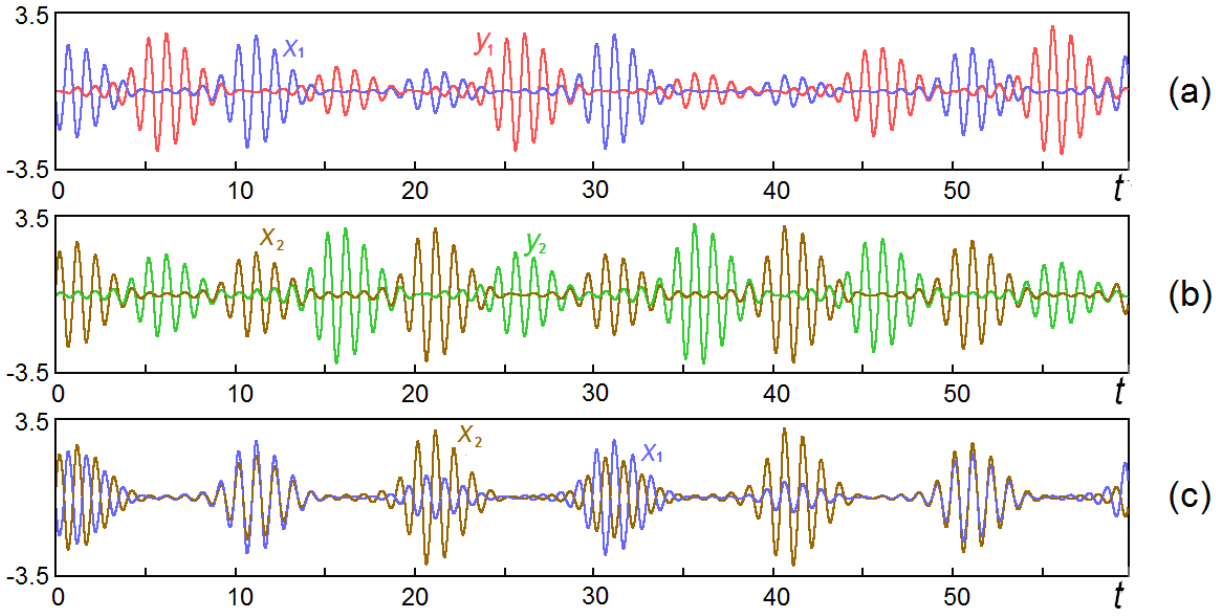

FIG. 5: (Color online) Waveforms generated by the system (7) for $A = 3$, $T = 10$, $\varepsilon = 0.06$, $\omega_0 = 2\pi$.

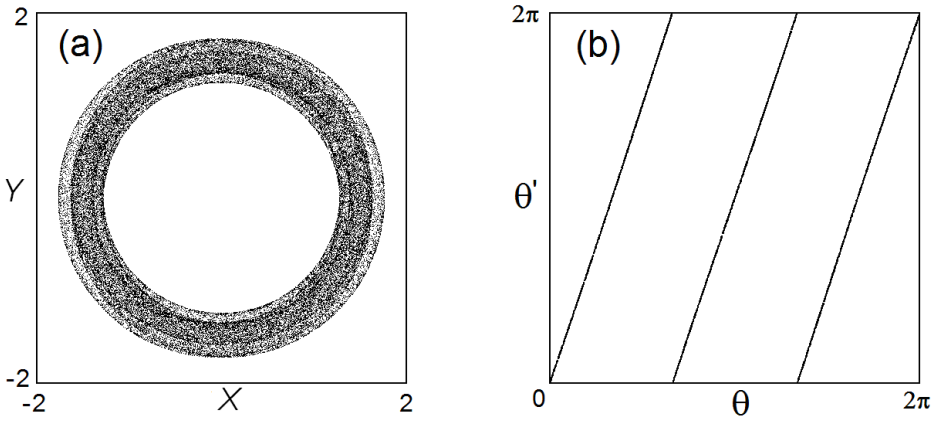

FIG. 6: Portrait of attractor in the Poincaré section in two-dimensional projection on the plane of the auxiliary variables introduced in the text and characterizing amplitudes of the first two oscillators (a) and diagram for the angular variables at successive instants $t = nT$ (b) for the system (7) at $A = 3$, $T = 10$, $\varepsilon = 0.06$, $\omega_0 = 2\pi$.

the axes on the diagram for the angular coordinate.

Figure 6 shows a portrait of the attractor in the Poincaré section on the plane of variables X, Y (panel (a)) and the iteration diagram for the angular variable θ (panel (b)). In comparison with Fig. 2 the attractor portrait looks as a formation widened in direction transversal to the coils. It is, as mentioned above, because a system now has a slowly evolving phase variable. Nevertheless, some fine structure inherited from the Cantor-like arrangement of the solenoid is distinguishable on the plot. As to the diagram for the angular variable, due to its proper definition, the plot looks very similar to that of Fig. 2(b) associated with the true uniformly hyperbolic attractor. Hence, one may assert that the hyperbolic component actually exists and that its intrinsic structural stability is conserved in spite of the perturbations arising from the dynamics of the phase variable.

Figure 7 shows results of a computation of the spectrum of Lyapunov exponents for the Poincaré map of the system (7) plotted versus the modulation intensity at fixed values of the other parameters $T = 10$, $\varepsilon = 0.06$, $\omega_0 = 2\pi$ (a), versus the coupling parameter at fixed values of $A = 3$, $T = 10$, $\omega_0 = 2\pi$ (b) and versus the modulation period at fixed values of $A = 3$, $\varepsilon = 0.06$, $\omega_0 = 2\pi$ (c), Observe that the largest exponent remains close to $\ln 3$ in a wide parameter range. This confirms the robust nature of the motion associated with the hyperbolic component. The second exponent is indistinguishable from zero in the computations, and is obviously associated with the slow evolving phase variable. Other exponents are all negative. Particularly, at $A = 3$ we

obtain

$$\begin{array}{ll} \Lambda_1 = 1.099, & \Lambda_2 = 0.000, \\ \Lambda_3 = -3.373, & \Lambda_4 = -4.198, \\ \Lambda_5 = -6.326, & \Lambda_6 = -7.097, \\ \Lambda_7 = -11.041, & \Lambda_8 = -12.020. \end{array} \tag{8}$$

It is interesting to compare these values with the results for the uniformly hyperbolic attractor of the four-dimensional real-amplitude system. (We recall that the Eqs. (7) reduce to that system in the approximation of the slow-varying amplitudes, see Appendix.) As one can see the values of Λ_1, Λ_4, Λ_6, Λ_7 from the list (8) agree well with the values of Λ_1, Λ_2, Λ_3, Λ_4 from the list (5). Dimension of the attractor in the Poincaré map in the present case is estimated from the Kaplan–Yorke formula as $D = 2 + (\Lambda_1 + \Lambda_2)/|\Lambda_3| \approx 2.33$. The integer part is distinct from the estimate in the previous section because of the presence of the phase variable, and the fractional part is distinct because the exponent Λ_3 does not have an analog in the list (5).

IV. A MODEL OF TWO ALTERNATELY EXCITED PAIRS OF NON-RESONANT VAN DER POL OSCILLATORS

Let us examine another version of a system composed of van der Pol oscillators, which corresponds more closely to the original model (2), and is governed by the set of equations

$$\begin{array}{l} \ddot{x}_1 - [A\cos(2\pi t/T) - x_1^2 - \frac{1}{2}x_2^2]\dot{x}_1 + \omega_1^2 x_1 = \varepsilon\dot{y}_1, \\ \ddot{x}_2 - [A\cos(2\pi t/T) - \frac{1}{2}x_1^2 - x_2^2]\dot{x}_2 + \omega_2^2 x_2 = \varepsilon\dot{y}_2, \\ \ddot{y}_1 - [-A\cos(2\pi t/T) - y_1^2 - \frac{1}{2}y_2^2]\dot{y}_1 + \omega_1^2 y_1 = \varepsilon(x_1^2 - \frac{3}{2}x_2^2)\dot{x}_1, \\ \ddot{y}_2 - [-A\cos(2\pi t/T) - \frac{1}{2}y_1^2 - y_2^2]\dot{y}_2 + \omega_2^2 y_2 = \varepsilon(\frac{3}{2}x_1^2 - x_2^2)\dot{x}_2. \end{array} \tag{9}$$

Unlike model (7), the first and the second oscillator of the alternately excited subsystems are now characterized by different natural frequencies ω_1 and ω_2, which are assumed not to satisfy low-order resonant conditions. Next, the factors $1/2$ are introduced at some terms to ensure correspondence with the system (2) in the slow complex amplitude approach for the non-resonant situation (see Appendix). Nevertheless, the transfer of the excitation between the first and the second oscillators of each subsystem due to the coupling terms in the right-hand parts remains *resonant* as the natural frequencies coincide for the oscillators marked with the same subscript 1 or 2 in both subsystems. Operation of the system is similar to that considered in the context of the previous models. In an approximate description basing on the real amplitude equations (4), we have the hyperbolic attractor of Smale–Williams type in the stroboscopic map. Because of its structural stability, it is natural to expect that the robust chaotic dynamics of the amplitudes survive in the system (9) as well, although the attractor of the complete set of equations will relate to the partially hyperbolic class.

To illustrate the dynamics we select the parameters $A = 3$, $T = 10$, $\varepsilon = 0.06$, like in the previous sections. With respect to the natural frequencies ω_1 and ω_2, it is appropriate to choose them in a ratio given by two successive Fibonacci numbers to avoid at least low order resonances; concretely, we set $\omega_1 = 5\omega_0$, $\omega_2 = 8\omega_0$ with $\omega_0 = 2\pi$.

Figure 8 shows waveforms generated by the system as obtained from numerical solution of Eqs. (9). Panels (a) and (b) represent the plots for the generalized coordinates of the pair-wise coupled oscillators. The first and the second subsystems are active alternately, and the intensities of the oscillations vary on successive stages in a random-like fashion.

Like in the previous section, we must pay special attention to definition of appropriate angular variable to illustrate the link with the Smale–Williams attractor in the amplitude dynamics. Now, the definition must be designed to disregard two phase variables relating to the oscillators marked with subscripts 1 and 2, respectively. The following evaluation routine is appropriate. For $i = 1, 2$, if $|x_i| > |u_i|$, set $s_i = \mathrm{sgn}(x_i)$, otherwise, $s_i = \mathrm{sgn}(u_i)$. Then, before and after each step of the Poincaré map, evaluate $X = s_1\sqrt{x_1^2 + u_1^2}$, $Y = s_2\sqrt{x_2^2 + u_2^2}$ and $X' = s_1\sqrt{{x_1'}^2 + {u_1'}^2}$, $Y' = s_2\sqrt{{x_2'}^2 + {u_2'}^2}$, where the prime marks the updated variables. (The factors $s_{1,2}$ are identical in evaluation both of X, Y and X', Y'.) Finally, set $\theta = \arg(X + iY)$ and $\theta' = \arg(X' + iY')$.

Figure 9 shows portrait of the attractor in the Poincaré section on the plane of variables X, Y (panel (a)) and the iteration diagram for the angular variable θ (panel (b)). The attractor looks similar to that shown in Fig. 2 with a certain transversal widening occurring apparently because of the slow evolution of the phase variables. The diagram for the angular variable looks very similar to that of Fig. 2b associated with the uniformly hyperbolic Smale–Williams attractor.

Figure 10 shows Lyapunov exponents for the Poincaré map of the system (9) versus parameter A (panel (a)), versus parameter ε (panel (b)) and versus parameter T (panel (c)) at fixed values of the other parameters. Again,

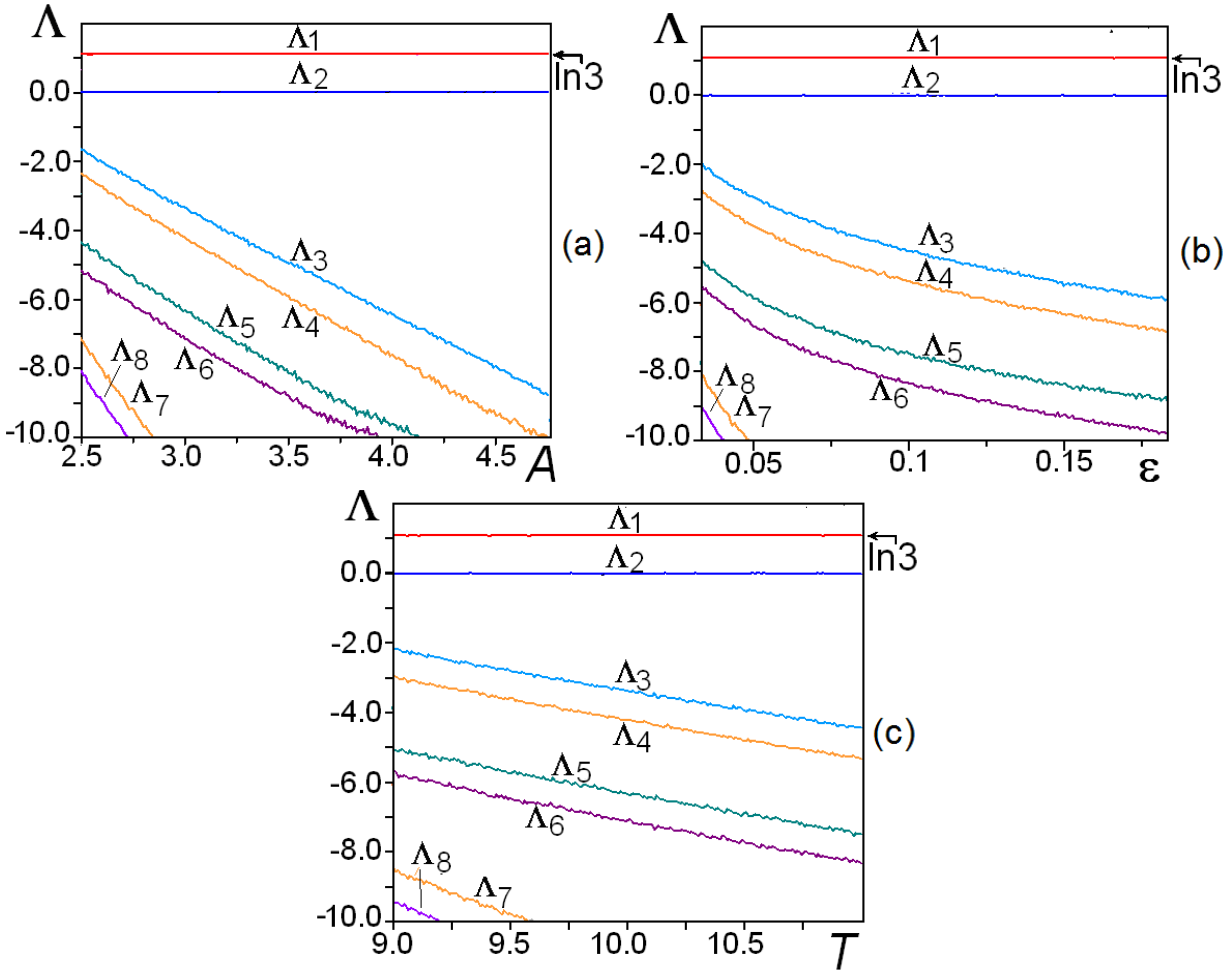

FIG. 7: (Color online) Lyapunov exponents of the Poincaré map for the system (7) plotted versus: (a) the amplitude of slow modulation A at fixed values of the other parameters $T = 10$, $\varepsilon = 0.06$, $\omega_0 = 2\pi$; (b) the coupling parameter ε at fixed values of $A = 3$, $T = 10$, $\omega_0 = 2\pi$; (c) the period of slow modulation T at fixed values of $A = 3$, $\varepsilon = 0.06$, $\omega_0 = 2\pi$.

the largest exponent is close to $\ln 3$ in a wide parameter range. The second and the third exponents are nearly zero being associated obviously with two slow evolving phase variables. Other exponents are all negative. Particularly, for $A = 3$, $T = 10$, $\varepsilon = 0.06$ we have

$$\begin{array}{ll} \Lambda_1 = 1.081, & \Lambda_2 = 0.000, \\ \Lambda_3 = 0.000, & \Lambda_4 = -4.173, \\ \Lambda_5 = -5.385, & \Lambda_6 = -5.386, \\ \Lambda_7 = -7.717, & \Lambda_8 = -10.632. \end{array} \qquad (10)$$

These results are remarkable close to the data (6) corresponding to the description of the system in terms of slow complex amplitudes. The Kaplan–Yorke estimate of the dimension is $D \approx 3.26$.

V. CONCLUSION

In this article we have advanced a new approach to the design of systems with attractor of Smale–Williams type in the stroboscopic map for the amplitudes of oscillators constituting the system. The approach is based on the manipulation by the angular variable describing distribution of amplitudes for self-oscillators, which are fed from a common supply of energy. By this manipulation the angular variable undergoes transformation according to expanding circle map on each time period of the externally forced periodic parameter modulation. The proposed principle can be implemented e.g. in systems of electronics and nonlinear optics for the generation of robust chaos. Moreover, on this principle, one can built many models manifesting various interesting phenomena of complex dynamics, like it was done with systems based on manipulation by phases of successively generated oscillatory trains (Arnold cat map dynamics [25, 37], complex analytic dynamics with Mandelbrot and Julia sets [38], robust strange nonchaotic attractor [39], etc.).

A subtle point in the present study is that the feasible examples composed of van der Pol oscillators and discussed in Section II and III are reduced to the equation

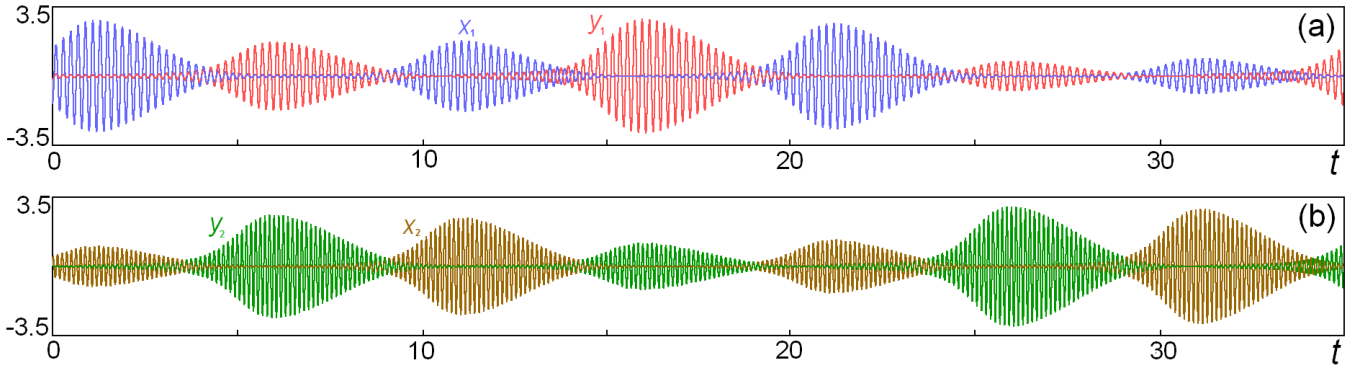

FIG. 8: (Color online) Typical pattern of time dependences for coordinate variables of four oscillators obtained from numerical solution of Eqs. (9) at $T = 10$, $A = 3$, $\varepsilon = 0.06$, $\omega_1 = 10\pi$, $\omega_2 = 16\pi$.

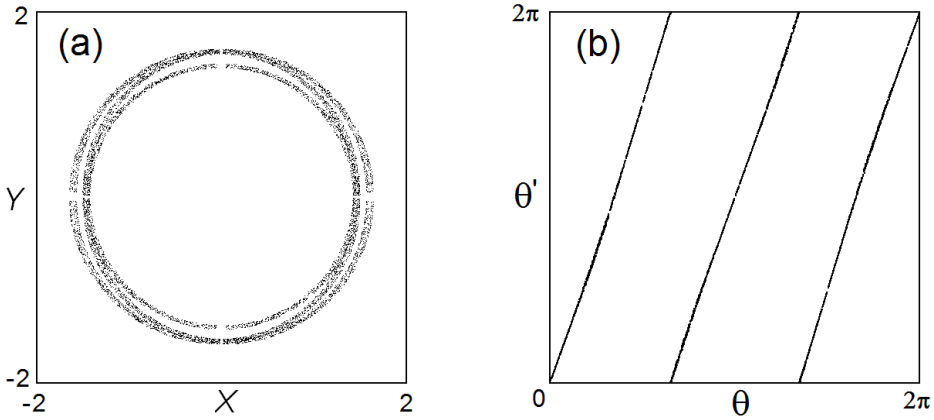

FIG. 9: (a) Portrait of attractor in the Poincaré section in two-dimensional projection on the plane of two real variables relating to the first two oscillators of the system (9) (see text). (b) Diagram for the angular variables for the system (9). Parameters are $T = 10$, $\varepsilon = 0.06$, $A = 3$, $\omega_1 = 10\pi$, $\omega_2 = 16\pi$.

with a uniformly hyperbolic attractor only in a certain approximation corresponding to the description in terms of real amplitudes while neglecting the phases. When the phases are taken into account, the attractor in principle has to be regarded as belonging to the class of partially hyperbolic attractors. Nevertheless, because of the structural stability for the attractor of the amplitude equations, it is natural to expect that the dynamics of the amplitudes is not affected by influence of the dynamics of the phases, and therefore this dynamics preserves the properties intrinsic to the uniformly hyperbolic attractor. Data of numerical simulations seem to confirm this assumption, but a mathematical justification would, of course, be desirable.

In this frame, it is worth noting that elaboration of the mathematically sound criteria for partial hyperbolicity, which would allow verification through computations (like the cone criterion, or analysis of the distribution of angles of intersection of stable and unstable subspaces for the uniform hyperbolicity) surely deserves attention as well as the question to what extent physically meaningful roughness of chaotic dynamics may be associated with the partially hyperbolic attractors.

In any case, the material presented in this article is of practical interest in a frame of design of robust chaos generators e.g. for communication systems, cryptography, random number generation. At the same time it is of theoretical interest by providing deep and well-developed concepts of the mathematical hyperbolic theory with a physical content.

Acknowledgement

O.B.I. acknowledges partial support from Grant of President of Russian Federation MK-905.2010.2, and S.P.K. acknowledges partial support from RFBR grant No 09-02-00426.

VI. APPENDIX: THE SLOW-AMPLITUDE DESCRIPTION OF THE MODELS COMPOSED OF THE VAN DER POL OSCILLATORS

Let us apply the method of slow complex amplitudes [2, 22, 40, 41] first to the system (9). With this,

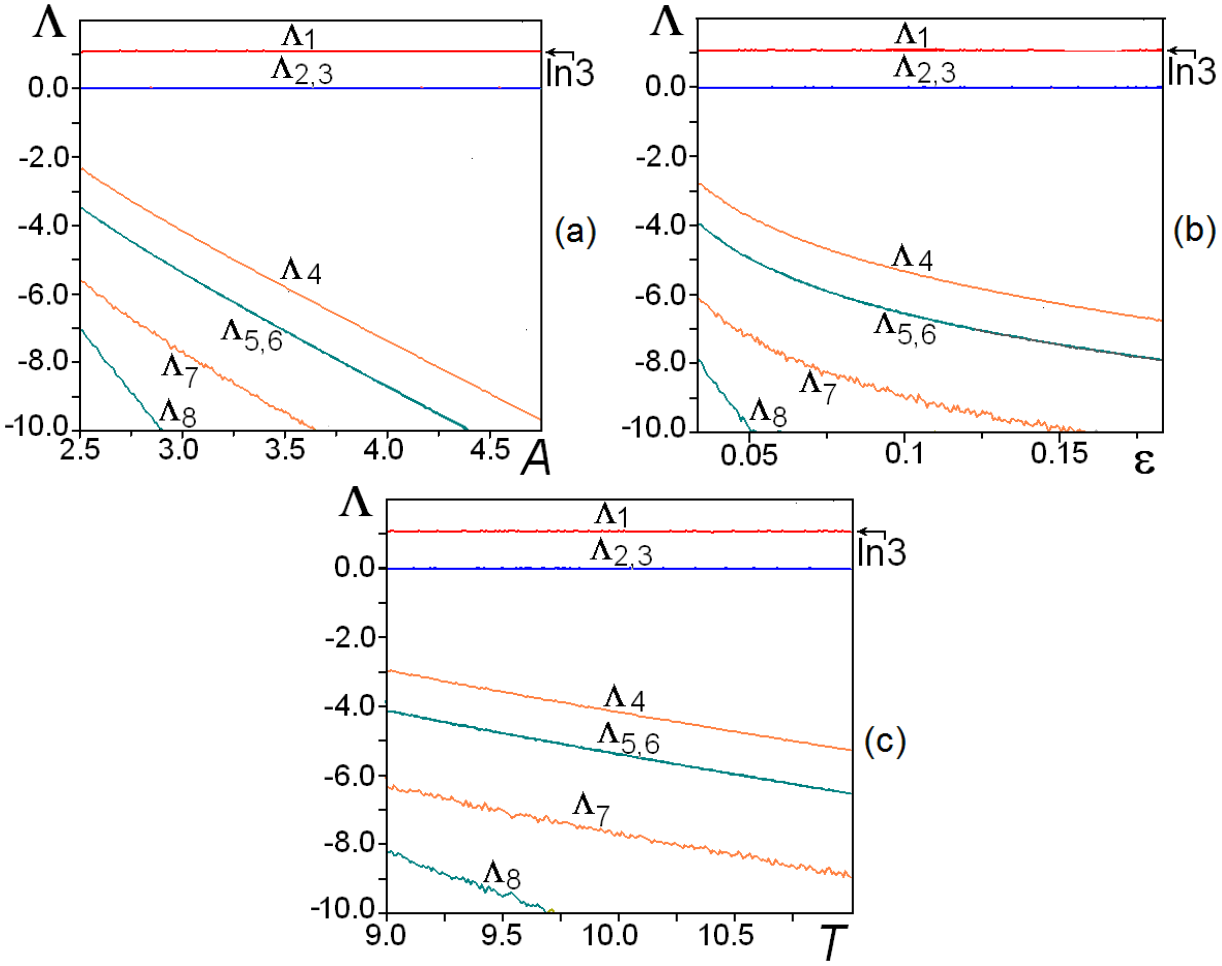

FIG. 10: (Color online) Lyapunov exponents of the Poincaré map for the system (9) plotted versus: (a) the amplitude of slow modulation A at fixed values of $T = 10$, $\varepsilon = 0.06$; (b) the coupling parameter ε at fixed values of $A = 3$, $T = 10$; (c) the period of slow modulation T at fixed values of $A = 3$, $\varepsilon = 0.06$. The values of the other parameters are $\omega_1 = 10\pi$, $\omega_2 = 16\pi$.

purpose we set

$$\begin{aligned} x_1 &= a_1 e^{i\omega_1 t} + a_1^* e^{-i\omega_1 t}, \\ x_2 &= a_2 e^{i\omega_2 t} + a_2^* e^{-i\omega_2 t}, \\ y_1 &= b_1 e^{i\omega_1 t} + b_1^* e^{-i\omega_1 t}. \\ y_2 &= b_2 e^{i\omega_2 t} + b_2^* e^{-i\omega_2 t}, \end{aligned} \tag{11}$$

and

$$\begin{aligned} \dot{x}_1 &= i\omega_1 a_1 e^{i\omega_1 t} - i\omega_1 a_1^* e^{-i\omega_1 t}, \\ \dot{x}_2 &= i\omega_2 a_2 e^{i\omega_2 t} - i\omega_2 a_2^* e^{-i\omega_2 t}, \\ \dot{y}_1 &= i\omega_1 b_1 e^{i\omega_1 t} - i\omega_1 b_1^* e^{-i\omega_1 t}, \\ \dot{y}_2 &= i\omega_2 b_2 e^{i\omega_2 t} - i\omega_2 b_2^* e^{-i\omega_2 t}. \end{aligned} \tag{12}$$

where complex amplitudes $a_{1,2}(t)$, $b_{1,2}(t)$ are assumed to be functions of time. Simultaneous validity of (11) and (12) implies that the following relations must take place

$$\begin{aligned} \dot{a}_1 e^{i\omega_1 t} + \dot{a}_1^* e^{-i\omega_1 t} &= 0, \\ \dot{a}_2 e^{i\omega_2 t} + \dot{a}_2^* e^{-i\omega_2 t} &= 0, \\ \dot{b}_1 e^{i\omega_1 t} + \dot{b}_1^* e^{-i\omega_1 t} &= 0, \\ \dot{b}_2 e^{i\omega_2 t} + \dot{b}_2^* e^{-i\omega_2 t} &= 0. \end{aligned} \tag{13}$$

(Acceptance of these relations is rightful: as we introduce four complex variables instead of four real ones, we are free to impose these additional conditions.)

Now, we substitute the variables x and y expressed in terms of the complex amplitudes in Eqs. (9) and, accounting for the relations (13), replace the derivatives of the conjugate variables through the complex amplitudes themselves, e.g. $\dot{a}_1^* e^{-i\omega_1 t} = -\dot{a}_1 e^{i\omega_1 t}$ etc. The resulting set of equations is exact, but a cumbersome representation of the original equations in the new variables a_1, a_2, b_1, b_2. The next step is account for the slow-varying nature of the complex amplitudes. We multiply the equations for variables a_1 and b_1 by $e^{-i\omega_1 t}$, and the equations for a_2 and b_2 by $e^{-i\omega_2 t}$ and perform the averaging over the fast oscillations. In the absence of low-order resonances (relations of type $p\omega_1 = q\omega_2$ with integer coefficients less than 4), this corresponds simply to removing all terms in the equations containing the exponentials. After some obvious, though cumbersome algebraic manipulations, we obtain exactly the Eqs. (2) for the complex amplitudes a_1, a_2, b_1, b_2.

Let us finally consider the application of this method to Eqs. (7). Now, the natural frequencies of all oscillators are equal, and we use the relations (11)-(13) setting $\omega_{1,2} = \omega_0$. After substitution into Eqs. (7) one observes that some additional terms survive in the averaged relations because of the equality of the frequencies, and the resulting set of equations reads

$$\begin{aligned}
\dot{a}_1 &= \tfrac{1}{2}\left[A\cos(2\pi t/T)a_1 - |a_1|^2 a_1 - 2|a_2|^2 a_1 + a_1^* a_2^2\right] + \tfrac{1}{2}\varepsilon b_1,\\
\dot{a}_2 &= \tfrac{1}{2}\left[A\cos(2\pi t/T)a_2 - 2|a_1|^2 a_2 + a_1^2 a_2^* - |a_2|^2 a_2\right] + \tfrac{1}{2}\varepsilon b_2,\\
\dot{b}_1 &= \tfrac{1}{2}\left[-A\cos(2\pi t/T)b_1 - |b_1|^2 b_1 - 2|b_2|^2 b_1 + b_1^* b_2^2\right] + \tfrac{1}{2}\varepsilon(|a_1|^2 a_1 - 6|a_2|^2 a_1 + 3a_1^* a_2^2),\\
\dot{b}_2 &= \tfrac{1}{2}\left[-A\cos(2\pi t/T)b_2 - 2|b_1|^2 b_2 + b_1^2 b_2^* - |b_2|^2 b_2\right] + \tfrac{1}{2}\varepsilon(6|a_1|^2 a_2 - 3a_1^2 a_2^* - |a_2|^2 a_2).
\end{aligned} \tag{14}$$

Note that these equations differ from the initial model (2). However, their structure allows us to consider a situation when all the amplitudes are real. With this additional assumption, the Eqs. (14) reduce precisely to the real-amplitude equations (4).

Lyapunov exponents computed for the attractor of the stroboscopic Poincaré map for the system (14) with $A = 3$, $T = 10$, $\varepsilon = 0.06$:

$$\begin{aligned}
&\Lambda_1 = 1.097, \quad &&\Lambda_2 = 0.000,\\
&\Lambda_3 = -3.414, \quad &&\Lambda_4 = -4.167,\\
&\Lambda_5 = -6.204, \quad &&\Lambda_6 = -7.584,\\
&\Lambda_7 = -10.834, \quad &&\Lambda_8 = -11.845
\end{aligned} \tag{15}$$

are found to be in remarkable agreement with the results (8). This confirms the applicability of the slow amplitude method in the operation modes we deal with.

[1] L. Glass and M.C. Mackey, *From Clocks to Chaos: The Rhythms of Life* (Prinston University Press, Prinston, 1988).

[2] M.I. Rabinovich, D.I. Trubetskov, *Oscillations and Waves in Linear and Nonlinear Systems* (Kluwer Academic Publisher, Dorderecht, Boston, London, 1989).

[3] S.K. Scott, *Chemical chaos* (Oxford University Press, Oxford, 1993).

[4] E. Mosekilde, *Topics in Nonlinear Dynamics: Applications to Physics, Biology, and Economic Systems* (World Scientific, Singapore, 1998).

[5] V.S. Anishchenko, *Nonlinear dynamics of chaotic and stochastic systems: tutorial and modern developments* (Springer, Berlin, 2002).

[6] J.W. Haefner, *Modeling biological systems: principles and applications* (Springer, Berlin, 2005).

[7] A. Loskutov, Physics-Uspekhi **53**, 1257 (2010).

[8] S. Smale, Bull. Amer. Math. Soc. (NS) **73**, 747 (1967).

[9] R.F. Williams, Publications mathématiques de l'I.H.É.S. **43**, 169 (1974).

[10] D.V. Anosov, G.G. Gould, S.K. Aranson, V.Z. Grines, R.V. Plykin, A.V. Safonov, E.A. Sataev, S.V. Shlyachkov, V.V. Solodov, A.N. Starkov, A.M. Stepin, *Dynamical Systems IX: Dynamical Systems with Hyperbolic Behaviour* in *Encyclopaedia of Mathematical Sciences*, Vol. 9 (Springer, Berlin, 1995).

[11] Y.G. Sinai, *Stochasticity of dynamical systems* in (A.V. Gaponov-Grekhov ed.) *Nolinear waves*, pp. 192–212 (Nauka, Moscow, 1979) (In Russian)

[12] R.V. Plykin, Math. USSR Sb. **23**(2), 233 (1974). (In Russian)

[13] L. Shilnikov, Int. J. of Bifurcation and Chaos **7**, 1353 (1997).

[14] A. Katok and B. Hasselblatt, *Introduction to the Modern Theory of Dynamical Systems* (Cambridge University Press, New York, 1995).

[15] V. Afraimovich and S.-B. Hsu, *Lectures on chaotic dynamical systems* (Somerville, MA, International Press, 2003).

[16] Ya.B. Pesin, *Lectures on partial hyperbolicity and stable ergodicity. Zurich lectures in advanced mathematics* (European Mathematical Society, 2004).

[17] T.J. Hunt and R.S. MacKay, Nonlinearity **16**, 1499 (2003).

[18] D. Ruelle and F. Takens, Commun. Math. Phys. **20**, 167 (1971).

[19] M. Benedicks and L. Carleson, Ann. of Math. **133**, (2), 73 (1991).

[20] C. Bonatti, L.J. Diaz, M. Viana, Dynamics Beyond Uniform Hyperbolicity. A Global Geometric and Probobalistic Perspective. *Encyclopedia of Mathematical Sciences*, Vol.102, (Springer, Berlin, 2005).

[21] V. Belykh. I. Belykh, E. Mosekilde, Int. J. of Bifurcation and Chaos **15**, 3567 (2005).

[22] A.A. Andronov, A.A. Vitt, S.Ė. Khaĭkin, *Theory of oscillators* (Pergamon Press, Oxford, 1966).

[23] S.P. Kuznetsov: Phys. Rev. Lett. **95**, 144101 (2005).

[24] S.P. Kuznetsov and E.P. Seleznev, J. Exper. Theor. Phys **102**, 355 (2006).

[25] S.P. Kuznetsov and A. Pikovsky, Physica D **232**, 87

(2007).
[26] L.V. Turukina and A. Pikovsky, Physics Letters A **375**(11), 1407 (2011).
[27] S.P. Kuznetsov and I.R. Sataev, Physics Letters A **365**, 97 (2007).
[28] D. Wilczak, SIAM J. Applied Dynamical Systems **9**, 1263 (2010).
[29] S. Banerjee, J.A. Yorke, C. Grebogi, Phys. Rev. Lett. **80**, 3049 (1998).
[30] Z. Elhadj and J.C. Sprott, Front. Phys. China **3**(2), 195 (2008).
[31] M. Drutarovský and P. Galajda, Radioengineering **16**(3), 120 (2007).
[32] G. Benettin, L. Galgani, A.Giorgilli, J.-M. Strelcyn, Meccanica **15**, 9 (1980).
[33] Y.-C. Lai, C. Grebogi, J.A. Yorke, I. Kan, Nonlinearity **6**, 779 (1993).
[34] Y. Hirata, K. Nozaki, T. Konishi, Prog. Theor. Phys. **102**, 701 (1999).
[35] V.S. Anishchenko, A.S. Kopeikin, J. Kurths, T.E. Vadivasova, G.I. Strelkova, Phys. Lett. A **270**, 301 (2000).
[36] P.V. Kuptsov and S.P. Kuznetsov, Phys. Rev. E **80**, 016205 (2009).
[37] O.B. Isaeva, A.Yu. Jalnine, S.P. Kuznetsov, Phys. Rev. E **74**, 046207 (2006).
[38] O.B. Isaeva, S.P. Kuznetsov, A.H. Osbaldestin, Physica D **237**, 873 (2008).
[39] A.Yu. Jalnine and S.P. Kuznetsov, Tech. Phys. **52**, 401 (2007).
[40] A.H. Nayfeh, *Perturbation Methods* (Wiley-VCH, Berlin, 2000).
[41] E. Grebenikov, Yu.A. Mitropolsky, Y.A. Ryabov, *Asymptotic Methods in Resonance Analytical Dynamics* (CRC Press, USA, 2004).